

Article

Analysis and Comparison of Multilayer Planar Structure Ultra–Wideband Absorbers for Visible to Mid–Infrared Light Using Different Simulation Software

Jing-Jenn Lin ¹, Ling-Chieh Tseng ², and Cheng-Fu Yang ^{2,3,*}

¹ Department of Applied Materials and Optoelectronic Engineering, National Chi Nan University, Nantou County 54561, Taiwan; cclin@nccu.edu.tw

² Department of Chemical and Materials Engineering, National University of Kaohsiung, Kaohsiung 811, Taiwan; jason8802178@gmail.com

³ Department of Aeronautical Engineering, Chaoyang University of Technology, Taichung 413, Taiwan

* Correspondence: cfyang@nuk.edu.tw

Received: Oct 3; Revised: Nov 3, 2023; Accepted: Nov 16, 2023; Published: Nov 28, 2023

Abstract: In the past, the featured finite difference time domain (FDTD) software was used to simulate a multilayer planar structure light absorber's design and obtain the optimal thickness for each layer through this software. In this study, we employed the thickness values obtained from FDTD in another software, COMSOL, for simulation. Subsequently, we compared the absorptivity simulated by COMSOL with that obtained through FDTD. Due to the different computational methods of the two software tools, the absorptivity simulated by COMSOL using the layer thickness values from FDTD became less accurate. As a result, the thickness of each layer was fine-tuned to identify the optimal parameters for each layer. The optimized parameters with the absorptivity values in the present study were compared to previous results. Variations in the optimal thickness for each layer when utilizing these two software applications were found with different results.

Keywords: FDTD software, COMSOL, Multilayer planar structure; Absorber

1. Introduction

In recent years, solar energy has been harnessed with various applications due to its inherent advantages, such as universality and security. We focused on two primary mechanisms for converting solar energy: solar-thermal and photovoltaic applications [1,2]. Incident solar light is converted into heat using various applications. In solar-thermal systems, the solar absorber is a critical component responsible for achieving optimal sunlight absorption across the entire solar spectrum. The absorber converts solar energy into other forms that can be readily used [3]. The applications of solar-thermal technology include industrial processes, including distillation, desalination, water purification, and others [4]. Additionally, using thermophotovoltaic (TPV) devices, the generated thermal energy is efficiently converted into electricity [5]. These devices effectively trap incident light within nanoscale spaces and dissipate it through the ohmic losses of the metal, resulting in a high absorption rate of incident light. Solar energy is harvested efficiently using plasmonic metamaterial absorbers [6]. Chen et al. introduced a dual-functional asymmetric plasmonic absorber designed for water purification and pollution detection with solar energy [4]. This development underscores the versatility of solar absorbers in addressing critical environmental and energy challenges.

The optical light interacts with nanostructured absorbers in nanoscale spaces to generate heat. As a consequence, a wide array of nanostructures based on metals is used to enhance light absorption. Cong et al. developed a broadband visible-light absorber through the hybridization of propagating surface plasmons (PSP). Their designed absorber achieved an impressive average absorption rate of nearly 90% within the visible spectrum, spanning 400 to 750 nm [7]. Aydin et al. developed plasmonic super-absorbers capable of effectively absorbing light from 400 to 700 nm, demonstrating a measured average absorption rate of 71% [8]. Tang et al. proposed a theoretical approach involving absorbers constructed from concentric multi-split-ring arrays, resulting in an outstanding average absorption rate of 97.2% at a wavelength of 585 to 800 nm [9]. These developments illustrate the ongoing efforts to enhance light absorption through novel nanostructured materials and designs, with applications spanning various areas of technology and science.

Numerical simulations are used to explore the absorption mechanisms within designed absorbers, with various software tools at the forefront of this endeavor. These include the finite difference time domain (FDTD) method [10,11] and Computer Simulation Technology Microwave Studio [12]. Among these, COMSOL Multiphysics® (COMSOL) stands out as a versatile simulation platform and one of the most frequently employed numerical analysis software tools. It computes the optical properties of nanophotonic devices designed for light absorption [13]. COMSOL Multiphysics® excels in handling the complete workflow of modeling and simulation such as importing material properties, defining geometries, and formulating the physics to encapsulate specific phenomena. The software then adeptly solves these models and post-processes the results, thereby generating accurate and insightful data. The utilization of advanced simulation software such as COMSOL underscores the importance of computational tools in the design and analysis of complex nanophotonic structures, contributing significantly to our understanding of absorption principles and their practical applications.

In this research, we employed the COMSOL simulation software for the design and simulation of an innovative ultra-wideband (UWB) absorber [14]. This designed absorber featured seven-layer continuous plane films. This multilayer structure introduced innovations including the incorporation of the top SiO₂ square cube which served a purpose as an anti-reflective film and the simultaneous excitation of the symmetric Fabry-Pérot (FP) cavity resonance within the absorber. We compared the simulated results of the proposed absorber by using the results obtained using FDTD and COMSOL simulations. When the simulation software was different, the simulation results were significantly different. By using COMSOL and these innovative design elements, we elucidated the absorption mechanisms and demonstrated the exceptional performance of the absorber, in absorbing a broad range of wavelengths simultaneously in the UWB spectrum. These findings hold promise for various applications, including photodetectors, solar energy harvesting, and sensors, where wideband light absorption and high absorptivity are essential.

2. Parameters and Methods

Fig. 1(a) depicts the structure of the proposed multilayer absorber, comprising a stack of six thin film layers. The multilayer dielectric film on the top showed high anti-reflective characteristics. The bottom Ti-SiO₂-Ti structure formed a Fabry-Pérot resonance cavity. Fig. 1(b) provides a cross-sectional view of the absorber, with h₁, h₂, h₃, h₄, h₅, and h₆ denoting the thickness of each layer. These layers corresponded to the Ti substrate, SiO₂ dielectric layer, Ti metal layer, TiO₂ dielectric layer, Al₂O₃ dielectric layer, and SiO₂ dielectric layer, respectively. We used the finite difference time domain (FDTD) method, the width of the square Ti substrate was 300 nm, and the respective layer thicknesses were set as follows: h₁ = 300 nm, h₂ = 89.88 nm, h₃ = 18.48 nm, h₄ = 40.51 nm, h₅ = 66.54 nm, and h₆ = 97.21 nm. This multilayer absorber was specifically designed to have functionality and the ability to absorb a broad spectrum of light efficiently. The fundamental principle of COMSOL involves the transformation of differential equations for engineering problems into integral equations. Through geometric discretization and interpolation of variables, these equations were approximated, ultimately resulting in a system of algebraic equations. This system was then encoded into a program and solved by the computer to find the unknown variables within the equations, followed by subsequent post-processing.

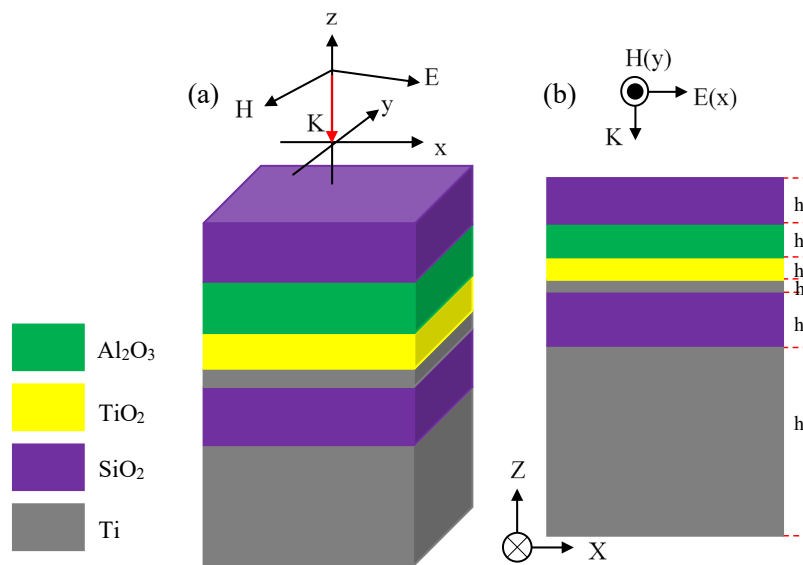


Fig. 1. Absorber Schematic. (a) 3D structure diagram and (b) cross-sectional view.

In the simulations, we imposed periodic boundary conditions in the x and y directions. The incident light was vertically oriented along the negative Z direction, with its polarization along the X -axis, facilitating the analysis. Due to the substantial thickness of the Ti substrate at the bottom, light could not penetrate, resulting in a zero transmittance for the structure. Therefore, the absorptivity was expressed as $A = 1 - R$, where R represents the reflectance. This approach effectively determined the absorptivity of the structure, given that no light passed through the Ti substrate. Fig. 2 shows the comparison of the absorptivity obtained through COMSOL simulation with the data referenced from the literature and simulated using the FDTD software. The graph illustrated that the absorptivity predicted by COMSOL was slightly lower when compared to those obtained from the FDTD simulation. This observation suggested a disparity in the absorptivity between the two simulation approaches. It is important to investigate and understand the specific reasons for this difference to refine the model and improve the accuracy of the COMSOL simulations. The comparative analysis result showed the enhancement of the reliability of the absorber's performance predictions and ensured their applicability in practical use cases.

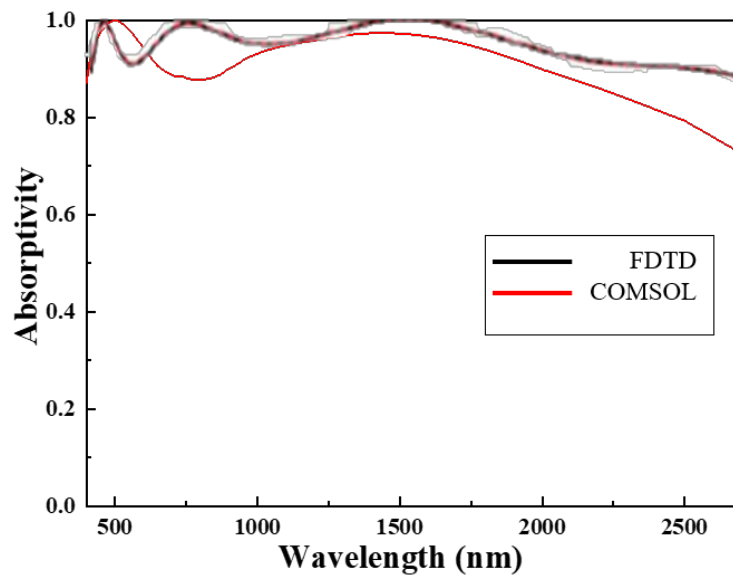


Fig. 2. Comparison of absorptivity between COMSOL and FDTD simulations.

3. Results and Discussion

Due to the different analysis and computation methods of these two software tools, we adjusted the thickness of each layer's materials using parameter sweeps to determine the optimal parameters for each layer. In Fig. 3(a), the absorptivity simulated for SiO_2 films with thickness ranging from 80–160 nm. In comparison to the original data with a thickness of 89.88 nm, it was found that the films with a thickness of 110 nm yielded better absorptivity. While there was a slight decrease in absorptivity within the wavelength range of 400–700 nm, there was a significant increase in absorptivity within 700–2700 nm (Fig. 3(b)). This adjustment and optimization of individual layer parameters were essential for fine-tuning the absorber's performance and aligning it with specific application requirements. They also demonstrated the capability of software tools and parameter exploration to enhance the efficiency of absorbers in a tailored manner. For the h3 layer of Ti, we adjusted the thickness of the h2 layer to 110 nm and performed a parameter sweep. The subsequent analysis for each layer followed a similar process. The simulated absorptivity for Ti films with thickness ranging from 10–50 nm was compared to that of the original 18.48 nm (Fig. 3(c)). The film of a thickness of 15 nm improved absorptivity. Fig. 3(d) shows that there was a noticeable increase in absorptivity within the 500–1000 nm wavelength range, enhancing absorptivity. For the h4 layer of TiO_2 , the simulated absorptivity for TiO_2 films with thickness ranging from 20–100 nm was compared to that of the original 40.51 nm (Fig. 3(e)). The film of a thickness of 60 nm showed superior absorptivity. Figure 3(f) illustrates that with a decrease in absorptivity within 800–1700 nm, there was also an increase in absorptivity within 600–800 nm and 1700–2700 nm (Fig. 3(f)). Thus, optimizing layer thicknesses through parameter scans was found to be essential in fine-tuning the absorber's performance as the absorber tailored the absorber's characteristics to specific wavelength ranges for applications of photodetectors and solar energy harvesting. We paid attention to the effectiveness of these parameter adjustments in achieving the desired performance outcomes. For the h5 layer of Al_2O_3 , the absorptivity was simulated for Al_2O_3 films with a thickness of 40–100 nm (Fig. 3(g)). Interestingly, there was not a significant difference in absorptivity when compared to the original thickness. Consequently, the original parameters were retained without any adjustments. For the h6 layer of SiO_2 , the simulated

absorptivity of SiO₂ films with a thickness of 50–150 nm was compared (Fig. 3(h)). Similar to other layers, there was not a substantial difference in absorptivity compared to the film of the original thickness. Thus, the original parameters were retained without any modifications. For the h5 and h6 layers, the original thickness was more effective in achieving the desired absorptivity without adjustment. The process of layer-by-layer optimization is important in customizing the absorber's design to maximize its efficiency in specific wavelength ranges with appropriate parameters.

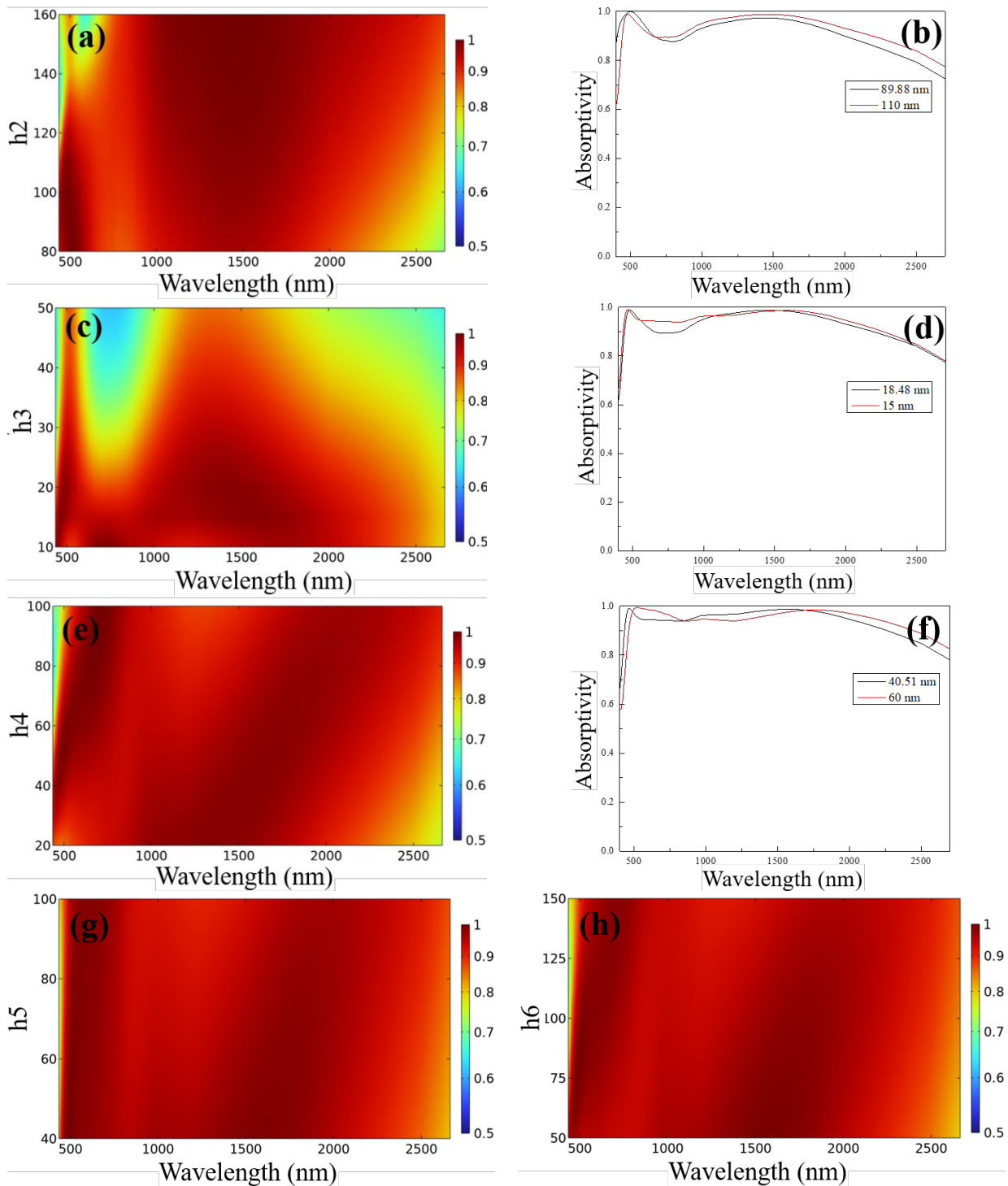


Fig. 3. Effects of different thicknesses on the absorptivity or absorption spectrum of each layer of the designed absorber. h2 SiO₂ layer on the (a) absorptivity and (b) absorption spectrum, h3 layer on the (c) absorptivity and (d) absorption spectrum, h4 TiO₂ layer on the (e) absorptivity and (f) absorption spectrum, and (g) h5 Al₂O₃ layer and (h) h6 SiO₂ layer on their absorptivity.

The optimal parameters for the designed absorber were as follows: the width of the square Ti substrate was 300 nm, and the respective layer thicknesses were set as follows: $h_1 = 300$ nm, $h_2 = 110$ nm, $h_3 = 15$ nm, $h_4 = 60$ nm, $h_5 = 66.54$ nm, and $h_6 = 97.21$ nm. Figure 4 illustrates a comparison between the absorption rates calculated using the optimized parameters for each layer through COMSOL simulation and the FDTD data. There was a significant improvement in absorptivity compared to the original parameters. Within the wavelength range of 460 to 2500 nm, an average absorption rate was 96%. The result showed how the optimized parameters contributed to the enhanced absorption capabilities. The enhancement at specific wavelength ranges was observed by an average of 96%. This result is important for various applications, such as photovoltaics, optical coatings, and sensors, where high absorption efficiency is crucial. The result also validated the effectiveness of the simulation in achieving the desired performance and provided a solid foundation for further exploration and development of materials and devices for optical and photonic applications.

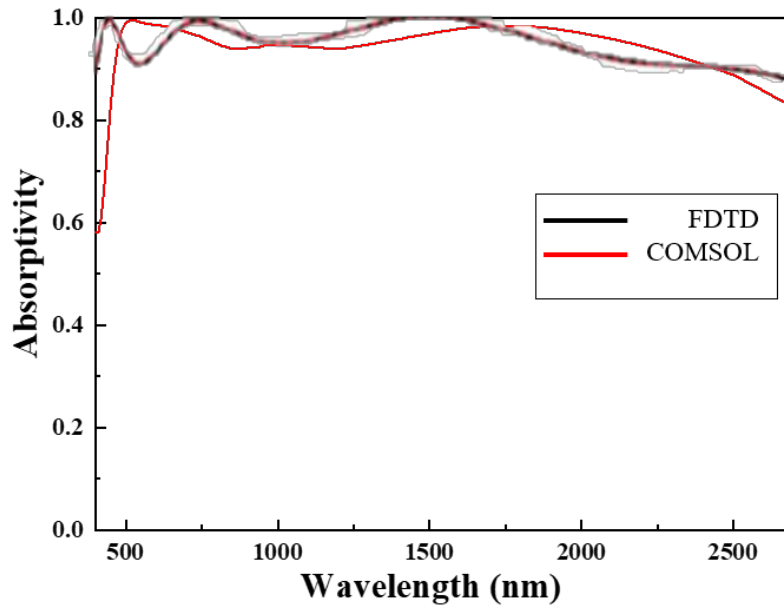


Fig. 4. Comparison of absorptivity between the optimized COMSOL and FDTD simulations.

The structure of this research was designed based on the Fabry-Perot resonance principle. We used a Ti-SiO₂-Ti configuration to create a Metal-Insulator-Metal (MIM) structure with the Fabry-Perot resonance cavity. As shown in Fig. 5, the simulated absorption spectrum revealed that in the wavelength range of 500–1300 nm, the MIM structure exhibited a prominent absorption peak of approximately 80%. Additionally, the electric field distribution in Fig. 6(a) at a wavelength of 500 nm showed the manifestation of the Fabry-Perot resonance within the SiO₂ layer of the MIM structure. With dielectric layers, a significant enhancement in absorption was achieved after the inclusion of a TiO₂ thin film. As depicted in Fig. 5, in the wavelength range of 500–1500 nm, the absorptivity exceeded 90%. This demonstrated that TiO₂ exhibited excellent absorption characteristics in the wavelength range. When combined with the electric field distribution shown in Figs. 6(a,b) at wavelengths of 500 nm and 1500 nm, the resonance within the TiO₂ layer occurred. Therefore, the addition of an Al₂O₃ thin film to form the Ti-SiO₂-Al₂O₃-Ti configuration increased the higher absorptivity than 90% in the wavelength range of 600–2000 nm. At around 1500 nm, the absorptivity reached 100%. The electric field distribution (Fig. 6(b)) at a wavelength of 1500 nm showed the resonant behavior of the Al₂O₃ film. With the Al₂O₃ thin film, the absorption peak became broader, and the wavelength at this peak was broadened. Finally, the incorporation of a SiO₂ thin film into the Ti-SiO₂-Al₂O₃-SiO₂-Ti configuration resulted in absorptivity exceeding 90% in the wavelength range of 500–2500 nm (Fig. 5). The electric field distribution in Figs. 6 (a–c) at wavelengths of 500, 1500, and 2500 nm showed the resonance characteristics within the topmost SiO₂ thin film. In summary, the structure based on the Fabry-Perot resonance cavity with the combination of Ti, TiO₂, Al₂O₃, and SiO₂ thin films resulted in a multi-layered MIM structure with remarkable absorption characteristics across a broad wavelength range. The addition of each dielectric layer enhanced the absorption, widened the absorption peak, and shifted the resonance to longer wavelengths, which is essential for various optical and photonic applications.

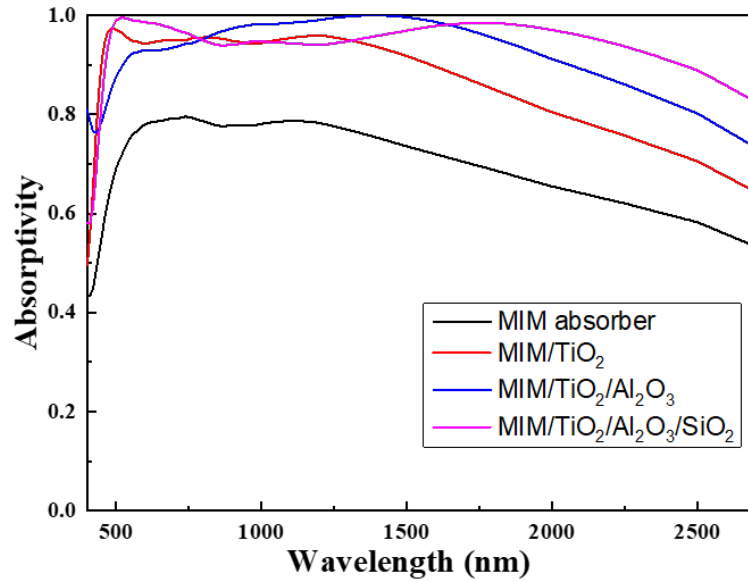


Fig. 5. Comparison of absorptivity for different materials covering the MIM absorber.

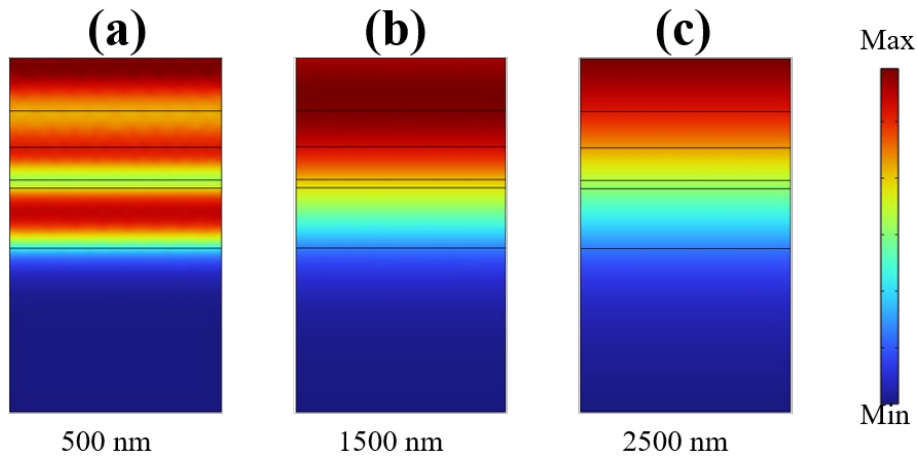


Fig. 6. Electric field distribution diagrams (a) 500 nm, (b) 1500 nm, and (c) 2500 nm.

The incident angle of light significantly influences the absorption rate. Figure 7 shows the simulated absorption spectra for Transverse Electric (TE) and Transverse Magnetic (TM) polarizations at incident angles ranging from 0 to 70°. Under TE polarization, as the incident angle increased to a substantial 50°, the absorptivity exceeded 90% in a wide wavelength range of 500–2700 nm. Similarly, under TM polarization, when the incident angle reached 50°, the absorption rate remained consistent above 90% in the wavelength range of 500–1700 nm. These distinct features highlighted the robustness of this absorber when exposed to larger incident angles. This insensitivity to incident angle variations is highly advantageous for practical applications as this absorber effectively captures and utilizes light when it arrives at non-normal angles. This makes the absorber appropriate for a variety of applications, especially when light incidence is not perfectly perpendicular to the surface. This property is also beneficial for solar energy harvesting which uses sunlight from various angles throughout the day.

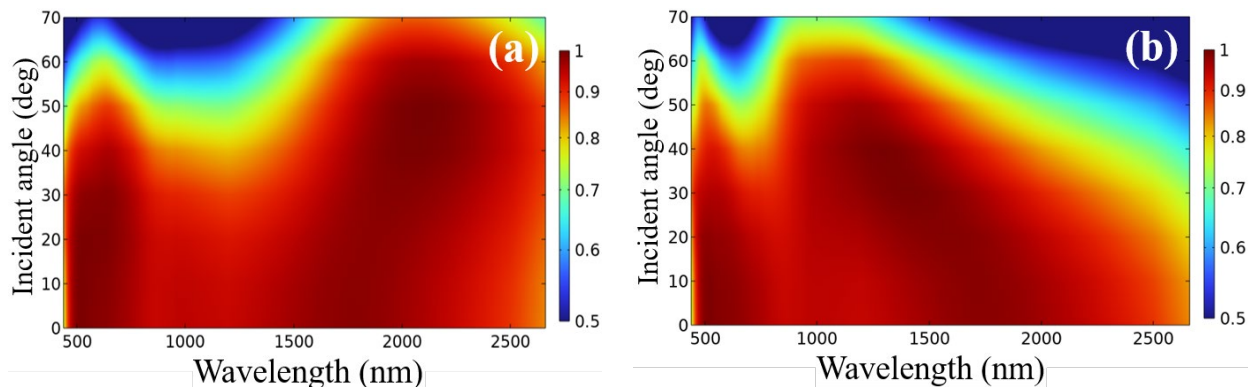


Fig. 7. Absorption spectra at various incident angles for (a) TE polarization and (b) TM polarization.

4. Conclusions

We developed an absorber with its peak performance through parameter optimization using COMSOL simulation software. The optimized parameters included a square Ti substrate with a width of 300 nm and the following layer thicknesses: $h_1 = 300$ nm, $h_2 = 110$ nm, $h_3 = 15$ nm, $h_4 = 60$ nm, $h_5 = 66.54$ nm, and $h_6 = 97.21$ nm. To refine the absorber's characteristics, three different layer configurations were adopted in dielectric layers within the symmetric Fabry-Pérot cavity resonance. The configurations included the Ti-SiO₂-Ti, Ti-SiO₂-Al₂O₃-Ti, and Ti-SiO₂-Al₂O₃-SiO₂-Ti configurations. The Ti-SiO₂-Al₂O₃-SiO₂-Ti configuration exhibited the most favorable absorber characteristics. Under TE polarization conditions, the absorber's remarkable performance was further demonstrated in the incident angle which increased to 50°. At this angle, the absorptivity exceeded 90% in the wavelength range of 500 to 2700 nm. This exceptional absorption performance underlines the practical viability and efficacy of the optimized design for a diverse range of applications.

Author Contributions: Conceptualization, J.-J. Lin and C.-F. Yang; methodology, J.-J. Lin, L.-C. Tseng and C.-F. Yang; software, J.-J. Lin, L.-C. Tseng and C.-F. Yang; validation, D. Yang, L.-C. Tseng and C.-F. Yang; formal analysis, J.-J. Lin, L.-C. Tseng and C.-F. Yang; data curation, J.-J. Lin, L.-C. Tseng and C.-F. Yang; writing—original draft preparation, J.-J. Lin and C.-F. Yang; writing—review and editing, J.-J. Lin and C.-F. Yang; visualization, J.-J. Lin, L.-C. Tseng and C.-F. Yang. All authors have read and agreed to the published version of the manuscript.

Acknowledgments: We would like to thank Pitotech Co. LTD for their help in teaching the use of COMSOL software.

Data Availability Statement: The data of this study are available from the corresponding author upon reasonable request.

Conflicts of Interest: The authors declare no conflict of interest.

References

- Chen, J.; Feng, J.; Li, Z.; Xu, P.; Wang, X.; Yin, W.; Wang, M.; Ge, X.; Yin, Y. Space-Confined Seeded Growth of Black Silver Nanostructures for Solar Steam Generation. *Nano Lett.* **2018**, *19*, 400–407.
- Embden, J.V.; Gaspera, E.D. Ultrathin Solar Absorber Layers of Silver Bismuth Sulfide from Molecular Precursors. *ACS Appl. Mater. Interfaces* **2019**, *11*, 16674–16682.
- Rephaeli, E.; Fan, S. Tungsten black absorber for solar light with wide angular operation range. *Appl. Phys. Lett.* **2008**, *92*, 211107.
- Chen, C.L.; Zhou, L.; Yu, J.Y.; Wang, Y.X.; Nie, S.M. Dual functional asymmetric plasmonic structures for solar water purification and pollution detection. *Nano Energy* **2018**, *51*, 451–456.
- Tan, F.; Wang, N.; Lei, D.Y.; Yu, W.; Zhang, X. Plasmonic Black Absorbers for Enhanced Photocurrent of Visible-Light Photocatalysis. *Adv. Opt. Mater.* **2017**, *5*, 1600399.
- Ryu, Y.; Kim, C.; Ahn, J.; Urbas, A.M.; Park, W.; Kim, K. Material-Versatile Ultrabroadband Light Absorber with Self-Aggregated Multiscale Funnel Structures. *ACS Appl. Mater. Interfaces* **2018**, *10*, 29884–29892.
- Cong, J.; Zhou, Z.; Yun, B.; Lv, L.; Yao, H.; Fu, Y.; Ren, N. Broadband visible-light absorber via hybridization of propagating surface plasmon. *Opt. Lett.* **2016**, *41*, 1965–1968.
- Aydin, K.; Ferry, V.E.; Briggs, R.M.; Atwater, H.A. Broadband polarization-independent resonant light absorption using ultrathin plasmonic super absorbers. *Nat. Commun.* **2011**, *2*, 1–7.
- Tang, B.; Zhu, Y.; Zhou, X.; Huang, L.; Lang, X. Wide-Angle Polarization-Independent Broadband Absorbers Based on Concentric Multisplit Ring Arrays. *IEEE Photon. J.* **2017**, *9*, 1–7.

10. Liu, J.; Ma, W.Z.; Chen, W.; Yu, G.X.; Chen, Y.S.; Deng, X.C.; Yang, C.F. Numerical analysis of a novel ultra-wideband metamaterial absorber with high absorptivity from visible light to near-infrared. *Opt. Express* **2020**, *28*, 23748–23760.
11. Chen, W.; Liu, J.; Ma, W.; Yu, G.X.; Chen, J.Q.; Cai, H.; Yang, C.F. Numerical Study of Multilayer Planar Film Structures for Ideal Absorption in the Entire Solar Spectrum. *Appl. Sci.* **2020**, *10*, 3276.
12. Xu, J.; Lin, C.H.; Chen, Y.T.; Tseng, H.W.; Wang, P.; Yang, C.F.; Lin, C.L. Design and Optimize a Red Color Reflector Using a Simulation Software. *Sens. Mater.* **2021**, *33*, 2619–2627.
13. Weng, C.E.; Yang, C.F.; Chen, Y.T.; Effect of Different Stacking Order of Ta₂O₅ and SiO₂ Films on the Reflective Properties of a Blue Distributed Bragg Reflector. *Mod. Phys. Lett. B* **2022**, *36*, 2242022.
14. Yang, D.; Tseng, L.C.; Li, W.Z.; Yang, C.F. Analysis of Ultra-Broadband Absorber with Multilayer Structure in Visible to Near Infrared Light. *Appl. Funct. Mater.* **2023**, *3*, 25–33.

Publisher's Note: IIKII stays neutral with regard to jurisdictional claims in published maps and institutional affiliations.



© 2023 The Author(s). Published with license by IIKII, Singapore. This is an Open Access article distributed under the terms of the [Creative Commons Attribution License](https://creativecommons.org/licenses/by/4.0/) (CC BY), which permits unrestricted use, distribution, and reproduction in any medium, provided the original author and source are credited.